Imaging Experiment of Multi-Pinhole Based X-Ray Fluorescence Computed Tomography Using Rat Head Phantoms

Tenta Sasaya, Tsuyoshi Oouchi, Tetsuya Yuasa
Graduate School of Science and Engineering
Yamagata University
Yonezawa, Japan

Seung-Jun Seo, Jae-Geun Jeon, Jong-Ki Kim
School of Medicine
Catholic University of Daegu
Daegu, Korea

Naoki Sunaguchi
Graduate School of Medicine
Nagoya University
Nagoya, Japan

Kazuyuki Hyodo
Institute of Materials Structure Science
High Energy Accelerator Organization (KEK)
Tsukuba, Japan

Tsutomu Zeniya
Graduate School of Science and Technology
Hirosaki University
Hirosaki, Japan

***Abstract*—Multi-pinhole based x-ray fluorescence computed tomography (mp-XFCT) delineates the spatial distribution of the non-radioactive agent in a living body by using fluorescent x-ray photons, which are emitted from the agent on de-excitation soon after extrinsic excitation and acquired with a multi-pinhole collimator and a 2-D detector. One of the potential applications is to image brain of small animals for development of treatment techniques and new drugs of brain disease in preclinical study. However, the measured photons are limited because a brain is covered with a skull which is a highly absorbing object. In this research, in order to investigate the applicability to brain imaging, we performed imaging experiments with phantoms to simulate a rat head using an actual mp-XFCT system, constructed at beamline AR-NE7A in KEK.**

Keywords— X-ray fluorescence computed tomography; pinhole; brain imaging; non-radioactive agent; image reconstruction

I. INTRODUCTION

Recently, the progress of genetic engineering accelerates preclinical studies for development of treatment techniques and new drugs, in which model small animals with a variety of diseases produced through genetic engineering are used. In those studies, nuclear medicine diagnostic equipment, such as positron emission tomography (PET) and single photon emission computed tomography (SPECT), are often employed to quantitatively and *in vivo* evaluate the function of target tissues or organs of model animal. However, nuclear medicine scan has some limitations that its spatial resolution is not high although its sensitivity is extremely high, and it must use radioisotope as imaging agent.

As a substitute imaging system easier to handle, XFCT has been developed, which is a hybrid technology between x-ray fluorescence analysis, which is one of the most sensitive physico-chemical analysis, and digital image processing technique of computed tomography [1-14]. The mp-XFCT improves the signal-to-noise ratio of the projection data by synthesizing the individual data from the multiple pinholes, compared to the single pinhole scheme [14]. From the viewpoint of CT, mp-XFCT is a type of emission CT, which delineates the distribution of non-radioactive agent using the x-ray photons, which are collected through a multi-pinhole collimator from among the fluorescent x-ray photons emitted from the agent in a 4π direction on de-excitation after extrinsic excitation [15,16].

Our interest lies in developing an imaging technique of small animal's brain for preclinical study of brain disease. Brain is covered with a skull which is a highly absorbing object. Therefore, the detected photons are limited. In this research, in order to investigate the applicability of mp-XFCT to brain imaging, we performed imaging experiments with phantoms to simulate a rat head using an actual mp-XFCT system constructed at beamline AR-NE7A in KEK. We prepared two kinds of phantoms. One was an acrylic cylinder including non-radioactive iodine, i.e., ^{127}I, whose circumference was covered with Al. The other was an actual rat skull including ^{127}I solution. We investigated the measurability of the objects covered with highly absorbing material using these phantoms.

978-9-0827-9703-9/19/$31.00

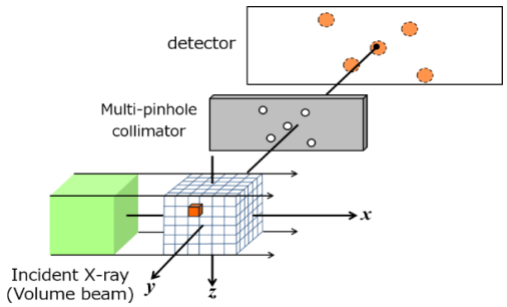

Fig. 1 Schematic of mp-XFCT.

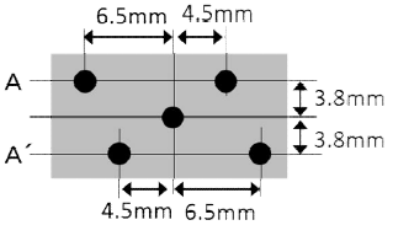

Fig. 2 Layout of multiple pinholes in the multi-pinhole collimator (top view).

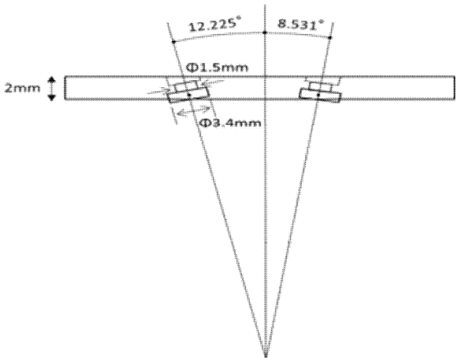

Fig. 3 Cross section of the multi-pinhole collimator at the "A" cross section drawn in Fig. 2.

II. METHOD

A. Imaging Method

Figure 1 shows a schematic diagram of the mp-XFCT imaging system [15]. An incident monochromatic volumetric beam with photon fluxes parallel to one another are linearly polarized within a horizontal plane, impinging and covering the object, which is placed around the origin. Imaging agents, e.g., I, Gd, and Au, are thus excited and then isotropically emit x-ray fluorescent photons on de-excitation. A multi-pinhole collimator, which is a thin plate with multiple pinholes (five pinholes in Fig. 1), and a 2-D detector are placed, such that the plate surface and the detective surface are parallel to the beam propagation. Only fluorescent photons passing through the pinholes are detected by the detector. For a single exposure, we obtain independent multiple projections (five projections in Fig. 1). Thus, the number of collected photons are increased. The projection acquisition is repeated while rotating the object over 360 degrees at a predefined angular step to finally obtain independent multiple sets of projections (five sets in Fig. 1).

B. Reconstruction Method

A reconstruction process is as follows: First, we consider the measurement process through a single pinhole. We introduce the index j (= 1, 2, …, N) to identify the voxels discretizing an object space, numbered in the lexicographic ordering in which N is the number of voxels, and the index i (= 1, 2, …, M) to identify the position of the individual detection elements in which the positions of detection elements throughout the whole projection acquisition are consecutively numbered, and M is the number of the positions. In these situation, the quantitative relationship for a single pinhole between the fluorescent photons measured at the ith detective position and the iodine concentration distributed at the individual voxels in the digitized object space is given as, $y_j = \Sigma_j p_{ij} \lambda_j$ (i = 1, 2, …, M), where y_i, λ_j, and p_{ij} are the number of the fluorescence photons counted at the ith position, the iodine concentration at the jth voxel and the constant of proportionality relating the iodine concentration at the jth voxel to the detected counts at the ith position, respectively; p_{ij} can be regarded as a conditional probability that y_i photons are counted at the ith detective position when iodine with concentration of λ_j exists in the jth voxel, and is given as a product of attenuation effects by an object, an incident beam flux, the photoelectric linear attenuation coefficient of iodine, the fluorescent yield of iodine, an exposure time, and the solid angle subtended by the jth voxel through the pinhole, which is able to be calculated in advance from the imaging geometry [14]. y_i and p_{ij} are known, and λ_j are unknown.

Since use of a multi-pinhole collimator produces projections for the individual pinholes, the above equation is rewritten as $y^k_j = \Sigma_j p^k_{ij} \lambda^k_j$ (i = 1, 2, …, M; k = 1. 2. …, L), where k is an index to identify the pinhole and L is the number of pinholes. As a result, we obtain a system of $M \times L$ linear equations. Then, we obtain L matrix equations $\mathbf{y}^k = \mathbf{P}^k \boldsymbol{\lambda}$ $(1 \le k \le L)$, where $\mathbf{y}^k = \left(y^k_1, y^k_2, \ldots, y^k_M\right)^T$, $\boldsymbol{\lambda} = \left(\lambda_1, \lambda_2, \ldots, \lambda_N\right)^T$, and $\mathbf{P}^k = (p^k_{ij})$. In addition, we introduce a K (= $L \times M$) -dimensional vector $\boldsymbol{\psi}$ and a $K \times N$ matrix $\boldsymbol{\Pi}$, where $\boldsymbol{\psi} = \left(\mathbf{y}^1, \mathbf{y}^2, \ldots, \mathbf{y}^L\right)^T$, and $\boldsymbol{\Pi} = \left(\mathbf{P}^{1T}, \mathbf{P}^{2T}, \ldots, \mathbf{P}^{LT}\right)^T$. As a result, our reconstruction leads to a linear inverse problem $\boldsymbol{\psi} = \boldsymbol{\Pi} \boldsymbol{\lambda}$, where vector $\boldsymbol{\psi}$ and matrix $\boldsymbol{\Pi}$ are known, and vector $\boldsymbol{\lambda}$ is to be estimated. For reconstruction, we straightforwardly apply the maximum likelihood - expectation maximization (ML-EM) algorithm to our linear inverse problem $\boldsymbol{\psi} = \boldsymbol{\Pi} \boldsymbol{\lambda}$ [15,16]. Actually, OS-EM (Ordered Subsets Expectation Maximization) algorithm [17] was used for solving the linear inverse problem $\boldsymbol{\psi} = \boldsymbol{\Pi} \boldsymbol{\lambda}$, which was implemented using C# on Windows 7. The number of subsets was 3; The number of

repetitions was 5. All the size of reconstructed images were 120 × 120 × 65, in which the edge length of a voxel was 0.172 mm.

III. Experiment

A. XFCT Imaging System

The mp-FXCT imaging system was constructed at the bending-magnet beamline AR-NE7A (6.5 GeV) in KEK. The mp-FXCT system was composed of a monochromator, a rotational stage for sample positioning, a multi-pinhole collimator, and a 2-D detector (Pilatus 100K with 487 × 195 elements (pixel size: 172 × 172 μm^2) manufactured by DECTRIS Ltd.). This detector was adopted because it measures at a high signal-to-noise ratio thanks to no dark current, and it also offers a higher data transmission rate than other types of 2-D detectors, such as CCD-based detector, although it has no sufficient energy resolution to discriminate the fluorescent x-ray photons from stray scattered x-ray photons in terms of their energies.

In this research, we paid attention to K-shell fluorescence of I (K_α: 28.3 keV). We by a double-crystal Bragg–Bragg monochromator using Si(111) single crystals selected the incident energy to 33.4 keV, which is just above the K-edge energy of I (33.2 keV), so that we can collect as many fluorescent photons as possible. The flux rate was about 9.3 × 10^7 photons/mm^2/s in front of the object. The cross section of the incident beam was collimated to 35 mm (horizontal) × 5 mm (vertical) by the slit. The distance between the rotational axis and the collimator plane, and between the collimator plane and the detector surface were 30.0 mm, and 30.0 mm, respectively. The rotational stage and the detector were controlled by a PC.

B. Multiple Pinholes Collimator with Sn Filter for Scatter Reduction

We fabricated a multi-pinhole collimator with five pinholes aligned as shown in Fig. 2. The collimator consisted of a 2-mm-thick Pb plate and five W pinhole tips. Figure 3 is a cross-section of the Pb plate at the level represented by "A" in Fig. 2. Five 1.5-mm-diameter holes were bored into the Pb plate so that their central axes were focused at a point 30 mm from the surface of the plate on the object side. Each hole had a 3.5-mm-diameter counterbore to enable the installation of a 3.4-mm-diameter W pinhole tip. The centres of the adjacent holes were arranged so that the projections acquired at 30 mm from

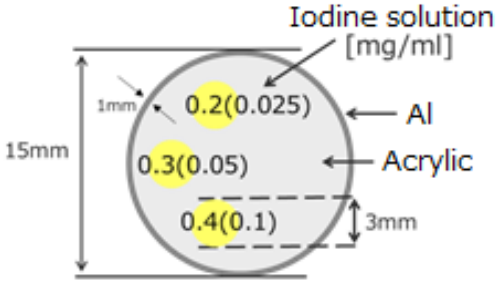

Fig. 4 Acrylic phantom covered with Al (top view)

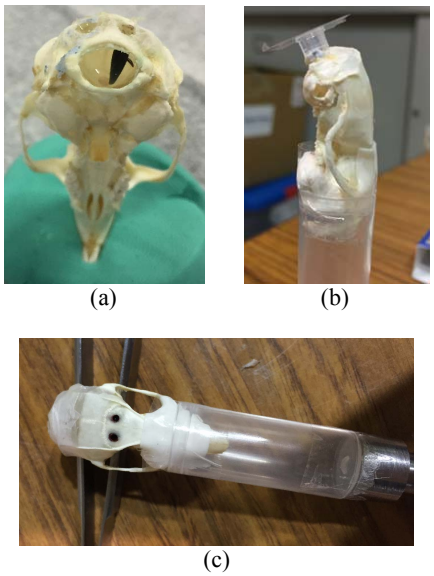

Fig. 5 Photographs of the rat skull phantom: (a) Front view, (b) side view, (c) top view.

the collimator plate would not overlap.

A thin film made of Sn of 0.15 mm in thickness was put on the surface of collimator so that the film covered the whole surface of collimator. The K-edge absorption energy of Sn is 29.2 keV. The photoelectric absorption coefficient behaves discontinuously at the K-edge; that is, it suddenly increases at incident energies just above the K-edge, whereas it monotonically decreases at energies below the K-edge. On the other hand, the energy of K_α-fluorescence of I are 28.3 keV. In our situation with an incident energy of 33.4 keV, many scattered photons whose energy are below 33.4 keV other than fluorescent x-ray photons are produced in an object. Thus, undesirable scattered photons pass through the pinholes to reach the detector. Since the detector used has no energy resolution to differentiate fluorescent photons from scattered photons, the measured data are contaminated and thereby the quality of reconstructed image is degraded. If we put a Sn-made thin film on the surface of collimator, it plays a role of a kind of filter for prevention of scatter contamination because ideally it intercepts scatter photons with energy higher than the K-edge of Sn of 29.2 keV but passes fluorescent photons of I with energy of 28.3 keV. However, the effect of the Sn filter is not complete. We will discuss its limit in the later section.

C. Phantoms

A physical phantom was an acrylic (PMMA) cylinder with 15 mm in diameter and 40 mm in height, which was covered with Al with 1 mm in thickness. It had three cavities with 3 mm in diameter and 15 mm in depth, which were filled with different concentration of I. Figure 4 shows the top view of the phantom. The other phantom was a rat skull including an I solution in the cerebral ventricle. Figure 5 are photographs of the phantom from several views. The acrylic phantom and the rat skull phantom were rotated at an angular step of 2° and 4° over 360°, respectively. The measurement time per projection were 180 s and 60 s for the acrylic phantom and for

the rat skull phantom, respectively. Namely, the number of projections for the former and for the latter were 180 and 90, respectively. Each phantom was measured two times while changing the concentration of I.

IV. Results

Figures 6(a) and (b) are a cross section of the reconstructed image of the acrylic phantom; The former had an I solution of relatively higher concentration than the latter. Although the concentration higher than 0.2 mg/ml was depicted, the concentration less or equal to 0.1 mg/ml could not be detected. The results show that the limit of detection of this phantom is 0.2 mg/ml. Figures 7(a) and (b) are reconstructed images of the rat skull phantom in MIP (Maximum Intensity Projection) representation; The former and the latter had I solution of 0.4 mg/ml and 0.2 mg/ml, respectively. In the both cases, the iodine regions are satisfactorily reconstructed. From the results, the iodine regions are satisfactorily reconstructed by mp-XFCT even if they are covered with a highly absorbing object, although the limit of detection decreases compared to the case without a highly absorbing cover.

V. Discussion

In the imaging system, we installed a Sn filter for prevention of scatter contamination in front of the multi-pinhole collimator. However, the experimental results in Figs. 6 and 7 show that the effect of the prevention filter is not sufficient. Scatter contamination leads to degradation of the quality of reconstructed image. To circumvent the difficulty, we can apply the dual-energy data acquisition which acquires two sets of projections at the incident energies just above and below the K-edge of the imaging agent and then reconstructs a three-dimensional image from projections based on the statistical model incorporating the scatter components [14]. Although the dual-energy data acquisition doubles the total measurement time, the difficulty can be overcome by replacing the detector with the state-of-the-art detector and increasing the number of pinholes.

VI. Conclusion

We investigated the feasibility of rat head imaging by an mp-XFCT using rat head phantoms. The experimental results demonstrated that mp-FXCT can satisfactorily reconstruct the I regions even if they are covered by a highly absorbing object, such as skull. The futuristic direction is to image a rat head with brain disease *in vivo*.

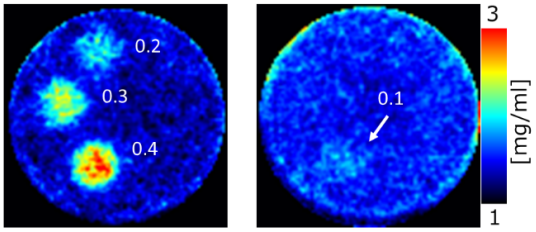

(a) (b)

Fig. 6 Reconstructed images of the acrylic phantom.

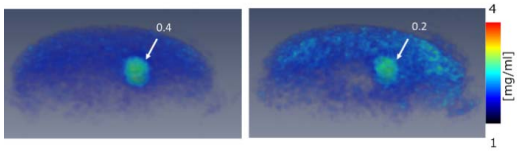

(a) (b)

Fig. 7 Reconstructed images of the rat skull phantom in MIP representation.

References

[1] R. Cesareo, and S. Mascarenhas, "A new tomographic device based on the detection of fluorescent X-rays," *Nucl. Instrum. Meth. A*, vol. 277 pp. 669-672, 1989.

[2] J. P. Hogan, R. A. Gonsalves, and A. S. Krieger, "Fluorescent computer tomography: A model for correction of X-ray absorption," *IEEE Trans. Nucl. Sci.*, vol. 38 pp. 1721-1727, 1991.

[3] G.-F. Rust, J. Weigelt, "X-ray fluorescent computer tomography with synchrotron radiation, " *IEEE Trans. Nucl. Sci.*, vol. 45, pp. 75-88, 1998.

[4] A. Simionovici, M. Chukalina, C. Schroer, M. Drakopoulos, A. Snigirev, I. Snigireva, B. Lengeler, K. Janssens, and F. Adams, "High-resolution X-ray fluorescence microtomography of homogeneous samples," *IEEE Trans. Nucl. Sci.*, vol. 47, pp. 2736-2740, 2000.

[5] C. G. Schroer, "Reconstructing x-ray fluorescence microtomograms," *Appl. Phys. Lett.*, vol. 79, pp. 1912-1914, 2001.

[6] P. J. La Riviere, J. Bian, and P. A. Vargas, "Penalized-likelihood sinogram restoration for computed tomography," IEEE Trans. Med. Imag., vol. 25, pp. 1022-1036, 2006.

[7] T. Yuasa, M. Akiba, et al., "Reconstruction method for fluorescent x-ray computed tomography by least squares method using singular value decomposition," *IEEE Trans. Nucl. Sci.*, vol. 44, pp. 54–62, 1997.

[8] T. Takeda, Q. Yu, et al., "Iodine imaging in thyroid by fluorescent X-ray CT with 0.05 mm spatial resolution," *Nucl. Instrum. Methods A*, vol. 467–468, pp. 1318-1321, 2001.

[9] Thet-Thet-Lwin, T. Takeda, et al., "Fatty Acid Metabolic Imaging by Fluorescent X-Ray Computed Tomography Imaging," *J. Synchrotron Radiat.*, vol. 14, pp. 158- 162, 2007.

[10] Thet-Thet-Lwin, T. Takeda, et al., "Visualization of age-dependent cardiomyopathic model hamster obtained by fluorescent X-ray computed tomography using I127-IMP," *J. Synchrotron Radiat.*, vol. 15, pp. 528-531, 2008.

[11] T. Takeda, J. Wu, et al., "X-ray fluorescent CT imaging of cerebral uptake of stable-iodine perfusion agent iodoamphetamine analog IMP in mice," *J. Synchrotron Radiat.*, vol. 16, pp. 57-62, 2009.

[12] Q. Huo, T. Yuasa, T. Akatsuka, et al., "Sheet-beam geometry for in vivo fluorescent x-ray computed tomography: proof-of-concept experiment in molecular imaging," *Opt. Lett.*, vol. 33, pp. 2494–2496, 2008.

[13] N. Sunaguchi, T. Yuasa, K. Hyodo, et al., "Fluorescent x-ray computed tomography using the pinhole effect for biomedical applications," *Opt. Comm.*, vol. 297, pp. 210–215, 2013.

[14] T. Sasaya, N. Sunaguchi, et al., "Dual-energy fluorescent x-ray computed tomography system with a pinhole design: Use of K-edge discontinuity for scatter correction," *Sci. Rep.*, vol. 7, 44143, 2017.

[15] T. Sasaya, N. Sunaguchi, et al., "Multi-pinhole fluorescent x-ray computed tomography for molecular imaging," *Sci. Rep.*, vol. **7**, 5742, 2017.

[16] T. Sasaya, N. Sunaguchi, et al., "Preliminary study on X-ray fluorescence computed tomography imaging of gold nanoparticles: Acceleration of data acquisition by multiple pinholes scheme," *Nucl. Instrum. Methods A* (in print) .

[17] H. M. Hudso, and R. S. Larkin, "Accelerated image reconstruction using ordered subsets of projection data," *IEEE Trans. Med. Imag.*, vol. 13, pp. 601-609, 1994.